Search for heavy resonances decaying into third generation quarks with the ATLAS detector

Josu Cantero (Oklahoma State University)

July 15, 2020

HEP seminar

Introduction

- Theories beyond the Standard Model (SM) involve enhanced symmetries that predict new gauge bosons, usually called W' or Z' bosons.
  - → Some models favor couplings of these new gauge bosons to third generation quarks.
  - → Good signal/background ratio thanks to *b*-tagging and top-tagging techniques.
  - → Complement searches using final states with first and second generation quarks.

→ This motivate searches for new heavy resonances:

1) W'→ tb (fully hadronic channel)
Phys. Lett. B 781 (2018) 327 (pdf)

2) Z'→ $b\bar{b}$
JHEP 03 (2020) 145 (pdf)

3) Z'→ $t\bar{t}$ (fully hadronic channel)
EXOT-2018-48 (pdf)

- **Outline:**

→ Jet reconstruction and calibration (arXiv:2007.02645)
→ Jet b-tagging (arXiv:1907.05120)
→ Jet substructure and top tagging (arXiv:1808.07858)
→ Analysis results

Jet reconstruction and calibration

- Jets are reconstructed using the anti-k_t algorithm with radius parameters $R = 0.4$ (small-R) and 1.0 (large-R).
- For use in jet reconstruction, calorimeter cells are first clustered into three-dimensional, massless, topological clusters using a nearest-neighbour algorithm.
  - → An event-by event correction to account for the position of the primary vertex in each event is applied to every topo-cluster.
- Jets reconstructed using only calorimeter-based energy information are referred to as EMTOPO jets.
- Hadronic final-state measurements can be improved by making more complete use of the information from both the tracking and calorimeter systems.
  - → Particle flow algorithm used. It combines information from the tracker and the calorimeter. Specifically, energy deposited in the calorimeter by charged particles is subtracted from the observed topo-clusters and replaced by the momenta of tracks that are matched to those topo-clusters → this improves energy and angular resolution, reconstruction efficiency, and pile-up stability compared to calorimeter jets.
  - → Jets reconstructed with PFLOW objects are referred to as PFLOW jets.
  - → Only available for jets with $R = 0.4$.

Jet reconstruction and calibration

- Jets need to be calibrated to restore the energy to that of jets reconstructed at particle level.
- This calibration is applied in different steps:
  - → pile-up corrections remove the excess energy due to additional proton–proton interactions.
  - → The absolute JES calibration to correct the jet so that it agrees in energy and direction with truth jets from the MC.
  - → Global sequential corrections to improve jet resolution and to remove the dependence on the flavour of the jet.
  - → In situ calibration to remove the remaining differences between data and MC simulation. It is derived using well-measured reference objects, including γ, Z bosons, and calibrated jets.

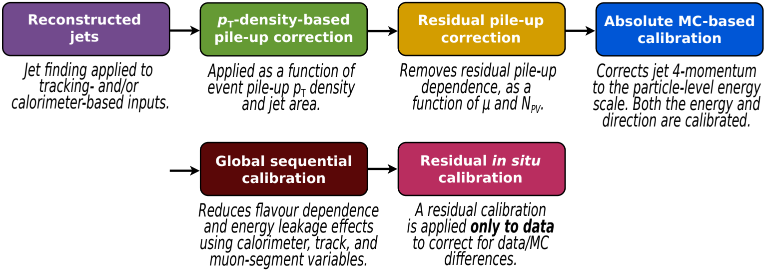

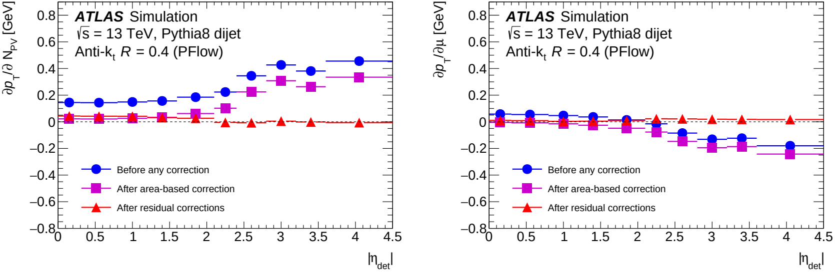

- The jet-area method uses to estimate the energy density (ρ) due to pile-up.
  - $\rightarrow$ $p_T^{corr} = p_T - \rho \times A - \alpha \times (N_{PV} - 1) - \beta \times \mu$
- The negative dependence on μ for out-of-time pile-up is a result of the liquid-argon calorimeter's pulse shape.
- Good stability of the p_T of the jet after all corrections.

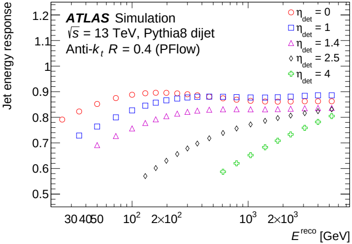

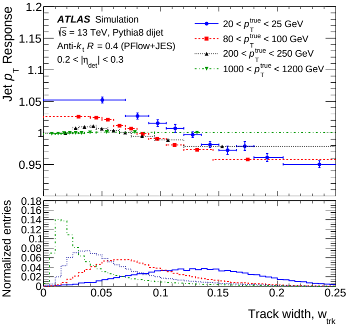

- The absolute JES correction corrects the reconstructed jet four-momentum accounting for non-compensating calorimeter response, energy losses in dead material and out-of-cone effects. $(\mathrm{R} = E_{\mathrm{reco}}/E_{\mathrm{true}})$
- The calibration is derived using a Pythia MC simulation of dijet events after the application of the pile-up corrections.
- After the JES correction, the response can vary from jet to jet depending on the flavour and energy distribution of the constituent particles.
  - → A quark-initiated jet includes hadrons with a higher fraction of the jet p_{T} that penetrate further into the calorimeter, while a gluon-initiated jet contains more particles of softer p_{T}, leading to a lower calorimeter response and a wider transverse profile.

Jet reconstruction and calibration

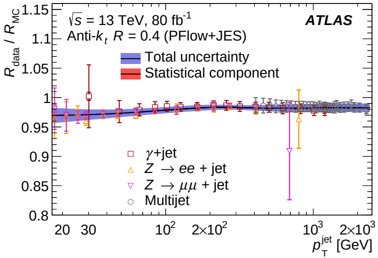

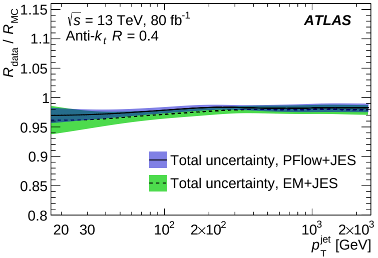

- One final calibration step to account for differences between the jet response in data and simulation causes by imperfect simulation of both the detector materials and the physics processes involved.
  - → Final in situ calibration measures the jet response in data and MC and uses the ratio as an additional correction in data: $c = \frac{R^{\text{data}}_{\text{in situ}}}{R^{\text{MC}}_{\text{in situ}}}$
- η intercalibration corrects the energy scale of forward ($0.8 < |\eta| < 4.5$) jets to match those of central ($|\eta| < 0.8$) jets using the p_{T} balance in dijet events.
- Z+jet and γ +jet analysis balance the hadronic recoil in an event against the p_{T} of a calibrated Z boson or γ.

Jet reconstruction and calibration

Component	Description
	η intercalibration
Systematic mis-modelling	Envelope of the generator, pile-up, and event topology variations
Statistical component	Statistical uncertainty (single component)
Non-closure	Three components describing non-closure at high energy and at $\eta \sim \pm 2.4$
Non-closure, 2018 only	Single component describing non-closure at $\eta \sim \pm 1.5$ due to Tile calibration
	Z + jet
Electron scale	Uncertainty in the electron energy scale
Electron resolution	Uncertainty in the electron energy resolution
Muon scale	Uncertainty in the muon momentum scale
Muon resolution (ID)	Uncertainty in muon momentum resolution in the ID
Muon resolution (MS)	Uncertainty in muon momentum resolution in the MS
MC generator	Difference between MC event generators
JVT cut	Jet vertex tagger uncertainty
$\Delta\phi$ cut	Variation of $\Delta\phi$ between the jet and Z boson
Subleading jet veto	Radiation suppression through second-jet veto
Showering & topology	Modelling energy flow and distribution in and around a jet
Statistical	Statistical uncertainty in 28 discrete p_T terms
	γ + jet
Photon scale	Uncertainty in the photon energy scale
Photon resolution	Uncertainty in the photon energy resolution
MC generator	Difference between MC event generators
JVT cut	Jet vertex tagger uncertainty
$\Delta\phi$ cut	Variation of $\Delta\phi$ between the jet and photon
Subleading jet veto	Radiation suppression through second-jet veto
Showering & topology	Modelling energy flow and distribution in and around a jet
Photon purity	Purity of sample used for γ + jet balance
Statistical	Statistical uncertainty in 16 discrete p_T terms
	Multijet balance
$\Delta\phi$ (lead, recoil system)	Angle between leading jet and recoil system
$\Delta\phi$ (lead, any sublead)	Angle between leading jet and closest subleading jet
MC generator	Difference between MC event generators
p_T^{asym} selection	Second jet's p_T contribution to the recoil system
Jet p_T	Jet p_T threshold
Statistical	Statistical uncertainty in 28 discrete p_T terms
	Pile-up
μ offset	Uncertainty in the μ modelling in MC simulation
N_{PV} offset	Uncertainty in the N_{PV} modelling in MC simulation
ρ topology	Uncertainty in the per-event p_T density modelling in MC simulation
p_T dependence	Uncertainty in the residual p_T dependence
	Jet flavour
Flavour composition	Uncertainty in the proportional sample composition of quarks and gluons
Flavour response	Uncertainty in the response of gluon-initiated jets
b-jets	Uncertainty in the response of b-quark-initiated jets
Punch-through	Uncertainty in GSC punch-through correction
Single-particle response	High-p_T jet uncertainty from single-particle and test-beam measurements
AFII non-closure	Difference in the absolute JES calibration for simulations in AFII

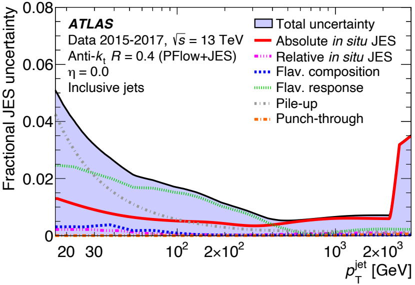

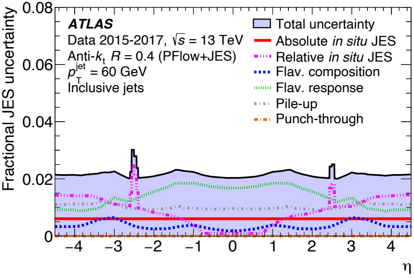

- 5% of uncertainty for $p_T \approx 20$ GeV. It decreases to 1% for $p_T \approx 200$ GeV and < 1% for 200 GeV < p_T < 2 TeV
  - → the high-p_T 'single particle' uncertainty is derived from studies of the response to individual hadrons and is used to cover the region beyond 2.4 TeV, where in-situ measurements no longer have statistical power.
- Uncertainty due to pile-up and jet flavor response dominates at low p_T.

Jet b-tagging

- The identification of jets containing *b*-hadrons (*b*-jets) against the large jet background containing *c*-hadrons but no *b*-hadron (*c*-jets) or containing neither *b*- or *c*-hadrons (light-flavour jets) is of major importance in many areas of the ATLAS physics programme.
  - → ATLAS uses various b-tagging algorithms. These algorithms exploit the long lifetime, high mass and high decay multiplicity of *b*-hadrons as well as the properties of the *b*-quark fragmentation.

- Performance of a *b*-tagging algorithm is characterised by the probability of tagging a *b*-jet and the probability of mistakenly identifying a *c*-jet or a light-flavour jet as a *b*-jet.

- Identification of *b*-jets based on:
  - → Track reconstructed in the ID with $p_{\mathrm{T}} > 500$ MeV and $|\eta| < 2.5$.
  - → Primary vertex reconstruction: displaced tracks from *b*-hadron decays selected using d_0 and z_0 (transverse and longitudinal impact parameters): low-level b-tagging algorithm IP3D.
  - → Secondary vertex consistent to *b*-hadron decay: low-level b-tagging algorithm SV1.
  - → Topological structure of weak *b*- and *c*-hadron decays inside the jet: low-level b-tagging algorithm JETFITTER .

- High level b-tagging algorithms such as MV2 (DL1) uses boosted decision trees (deep neural networks) combining the information previously listed.
  - → Mixed of $t\bar{t}$ and Z' samples used for the training

Jet b-tagging

Input	Variable	Description
Kinematics	p_T	Jet p_T
	η	Jet $\|\eta\|$
IP2D/IP3D	$\log(P_b/P_{\text{light}})$	Likelihood ratio between the b-jet and light-flavour jet hypotheses
	$\log(P_b/P_c)$	Likelihood ratio between the b- and c-jet hypotheses
	$\log(P_c/P_{\text{light}})$	Likelihood ratio between the c-jet and light-flavour jet hypotheses
SV1	$m(\text{SV})$	Invariant mass of tracks at the secondary vertex assuming pion mass
	$f_E(\text{SV})$	Energy fraction of the tracks associated with the secondary vertex
	$N_{\text{TrkAtVtx}}(\text{SV})$	Number of tracks used in the secondary vertex
	$N_{\text{2TrkVtx}}(\text{SV})$	Number of two-track vertex candidates
	$L_{xy}(\text{SV})$	Transverse distance between the primary and secondary vertex
	$L_{xyz}(\text{SV})$	Distance between the primary and the secondary vertex
	$S_{xyz}(\text{SV})$	Distance between the primary and the secondary vertex divided by its uncertainty
	$\Delta R(\vec{p}_{\text{jet}}, \vec{p}_{\text{vtx}})(\text{SV})$	ΔR between the jet axis and the direction of the secondary vertex relative to the primary vertex.
JetFitter	$m(\text{JF})$	Invariant mass of tracks from displaced vertices
	$f_E(\text{JF})$	Energy fraction of the tracks associated with the displaced vertices
	$\Delta R(\vec{p}_{\text{jet}}, \vec{p}_{\text{vtx}})(\text{JF})$	ΔR between jet axis and vectorial sum of momenta of all tracks attached to displaced vertices
	$S_{xyz}(\text{JF})$	Significance of average distance between PV and displaced vertices
	$N_{\text{TrkAtVtx}}(\text{JF})$	Number of tracks from multi-prong displaced vertices
	$N_{\text{2TrkVtx}}(\text{JF})$	Number of two-track vertex candidates (prior to decay chain fit)
	$N_{\text{1-trk vertices}}(\text{JF})$	Number of single-prong displaced vertices
	$N_{\geq 2\text{-trk vertices}}(\text{JF})$	Number of multi-prong displaced vertices
JetFitter c-tagging	$L_{xyz}(2^{\text{nd}}/3^{\text{rd}}\text{vtx})(\text{JF})$	Distance of 2^{nd} or 3^{rd} vertex from PV
	$L_{xy}(2^{\text{nd}}/3^{\text{rd}}\text{vtx})(\text{JF})$	Transverse displacement of the 2^{nd} or 3^{rd} vertex
	$m_{\text{Trk}}(2^{\text{nd}}/3^{\text{rd}}\text{vtx})(\text{JF})$	Invariant mass of tracks associated with 2^{nd} or 3^{rd} vertex
	$E_{\text{Trk}}(2^{\text{nd}}/3^{\text{rd}}\text{vtx})(\text{JF})$	Energy fraction of the tracks associated with 2^{nd} or 3^{rd} vertex
	$f_E(2^{\text{nd}}/3^{\text{rd}}\text{vtx})(\text{JF})$	Fraction of charged jet energy in 2^{nd} or 3^{rd} vertex
	$N_{\text{TrkAtVtx}}(2^{\text{nd}}/3^{\text{rd}}\text{vtx})(\text{JF})$	Number of tracks associated with 2^{nd} or 3^{rd} vertex
	$Y^{\text{min}}_{\text{trk}}, Y^{\text{max}}_{\text{trk}}, Y^{\text{avg}}_{\text{trk}}(2^{\text{nd}}/3^{\text{rd}}\text{vtx})(\text{JF})$	Min., max. and avg. track rapidity of tracks at 2^{nd} or 3^{rd} vertex

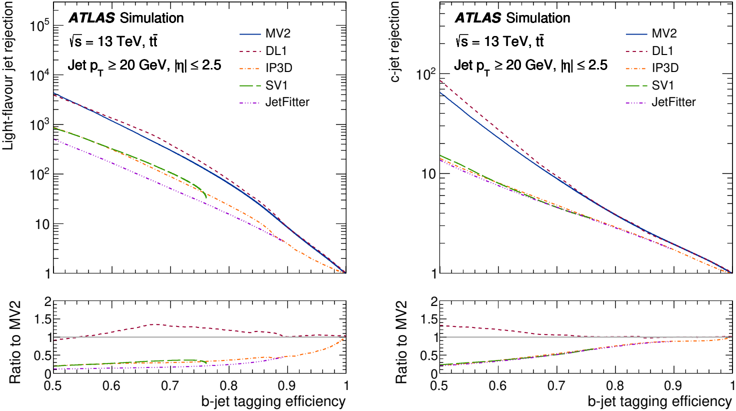

- Four WPs based on the efficiency of b-flavoured jets are derived: 60%, 70%, 77%, 85% WPs.
- Improvements in the light-flavour jet and *c*-jet rejections by factors of around 10 and 2.5 for high-level *b*-tagging algorithms at $\epsilon_{\mathrm{b}} = 70\%$.

- The performance of each *b*-tagging WP in the MC is corrected to the one observed in data.
  - → This is done by means of scale factors, SF $(p_{\mathrm{T}}, \eta) = \epsilon_{\mathrm{data}}(p_{\mathrm{T}}, \eta)/\epsilon_{\mathrm{MC}}(p_{\mathrm{T}}, \eta)$
- $t\bar{t}$ events in the di-lepton channel are selected in data and MC.
  - → High purity of *b*-flavoured jets.
  - → Events classified to extract flavour fractions: *bb*, *bl*, *ll*.
  - → *bb* flavour fraction used to extract ϵ_b in data and MC.

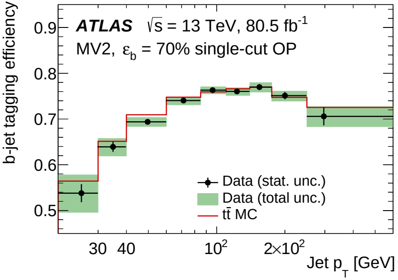

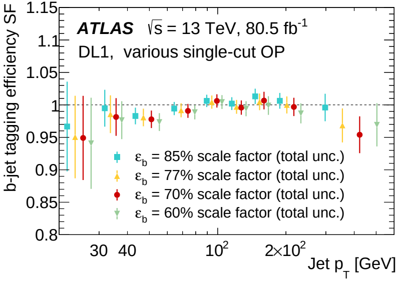

- Adequate description of ϵ_b by the MC.
- Similar SFs derived for each *b*-tagging WPs.

- Several different uncertainty sources considered.
  - → High p_{T} extrapolation uncertainties derived from MC to cover the high p_{T} region where data is not available.

MV2 70% WP:

Source of uncertainty	Relative uncertainty on ε_b [%] per jet p_{T} bin [GeV]								
	20–30	30–40	40–60	60–85	85–110	110–140	140–175	175–250	250–600
Data statistics	3.7	1.7	0.7	0.6	0.6	0.6	0.8	1.1	2.8
MC statistics	2.2	1.0	0.4	0.2	0.2	0.2	0.2	0.2	0.5
Jet energy scale	4.5	0.8	0.3	0.1	0.1	0.1	0.1	0.2	0.4
$t\bar{t}$ modelling	3.2	1.5	1.0	0.7	0.7	0.8	1.0	0.8	0.5
Single top modelling	2.5	0.5	0.6	0.6	0.4	0.3	0.3	0.4	1.1
Fake leptons modelling	1.8	1.1	0.1	0.2	< 0.1	< 0.1	0.2	< 0.1	0.2
Other sources	1.4	0.9	0.2	0.3	0.2	0.1	0.1	0.1	0.3
Total	7.7	3.0	1.4	1.1	1.0	1.1	1.3	1.5	3.1

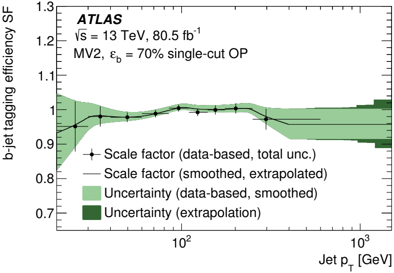

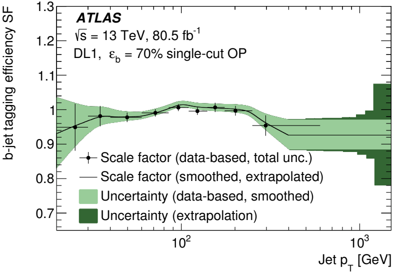

- Large-R jets ($R = 1.0$) using EMTopo objects as inputs.
  - → Since mass of Z, W and top larger than light quarks, a large radious jet is needed to collect all the decay products.
- Grooming technique used to remove the effects of pile-up and the underlaying event.
  - → Difference with respect to small-R jets. Larger effects expected since R is large.
  - → Trimming procedure in which original constituents of the jets are reclustered using the k_t algorithm with a radius parameter $R_{\mathrm{sub}} = 0.2$ to produce a collection of subjets. These subjets are then discarded if the p_T is less than 5% of the p_T of the original jet.
  - → Jet mass calibration (JMS) step included in the calibration chain of large-R jets. The rest similar to what is done for small-R jets.

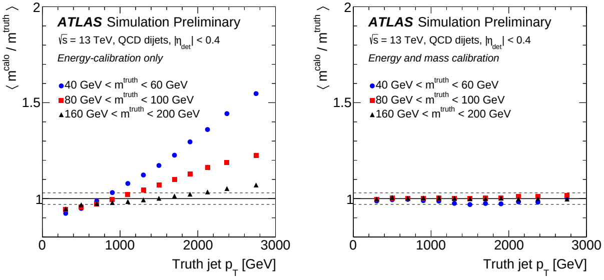

Jet substructure and top tagging

- From large-R jet constituents several observables can be defined to quantify a particular feature of the jet in an analytic way:
  - → jet mass.
  - → Splitting scales: d_{12}, d_{23} ...
  - → Energy correlation functions: C_2, D_2 ...
  - → N-subjettiness: τ_2, τ_3, τ_{32} ...

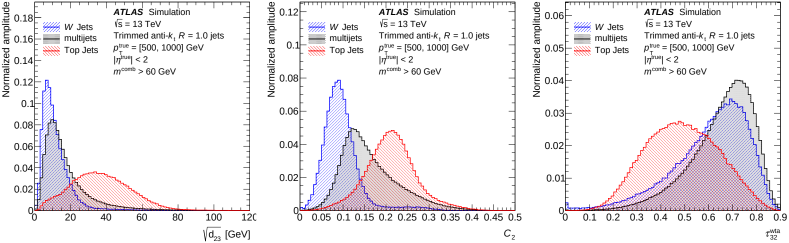

- These variables can be used to derive “low-level” W/top taggers or combined using multivariate classifiers (BDT, DNN ...) to derive “high-level” top taggers.
- Shower deconstruction: top-tagger based on the reconstruction of subjets to determine whether the subjet pattern is compatible with a parton shower profile typical of a top-quark decay.

Jet substructure and top tagging

- From large-R jet constituents several observables can be defined to quantify a particular feature of the jet in an analytic way:
  - → jet mass.
  - → Splitting scales: d_{12}, d_{23} ...
  - → Energy correlation functions: C_2, D_2 ...
  - → N-subjettiness: τ_2, τ_3, τ_{32} ...

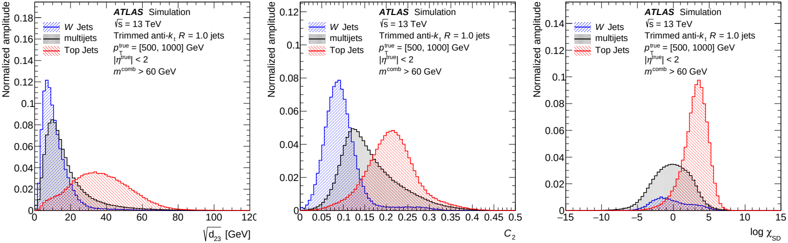

- These variables can be used to derive "low-level" W/top taggers or combined using multivariate classifiers (BDT, DNN ...) to derive "high-level" top taggers.
- Shower deconstruction: top-tagger based on the reconstruction of subjets to determine whether the subjet pattern is compatible with a parton shower profile typical of a top-quark decay.

Jet substructure and top tagging

	W Boson Tagging											Top Quark Tagging										
	DNN Test Groups									Chosen Inputs		DNN Test Groups									Chosen Inputs	
Observable	1	2	3	4	5	6	7	8	9	BDT	DNN	1	2	3	4	5	6	7	8	9	BDT	DNN
m^{comb}	○	○		○	○	○	○	○	○	○	○		○	○	○		○	○	○	○	○	○
p_T	○	○			○	○		○	○	○	○			○	○			○	○	○	○	○
e_3	○	○				○			○						○			○		○	○	○
C_2			○	○	○		○	○	○		○	○	○	○		○	○		○	○		○
D_2			○	○	○		○	○	○	○	○	○	○	○		○	○		○	○		○
τ_1	○	○				○			○	○					○			○		○		○
τ_2	○	○				○			○						○			○		○	○	○
τ_3															○			○		○		○
τ_{21}			○	○	○		○	○	○	○	○	○	○	○		○	○		○	○	○	○
τ_{32}												○	○	○		○	○		○	○	○	○
R_2^{FW}			○	○	○	○	○	○	○	○	○											
$\mathcal{P}$			○	○	○	○	○	○	○	○	○											
a_3			○	○	○	○	○	○	○	○	○											
A			○	○	○	○	○	○	○	○	○											
z_{cut}			○	○	○		○	○	○		○											
$\sqrt{d_{12}}$		○				○	○	○	○	○	○					○	○	○	○	○	○	○
$\sqrt{d_{23}}$																○	○	○	○	○	○	○
$KtDR$		○				○	○	○	○	○	○											
Q_w																○	○	○	○	○	○	○

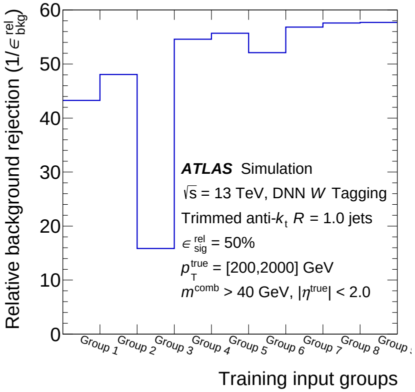

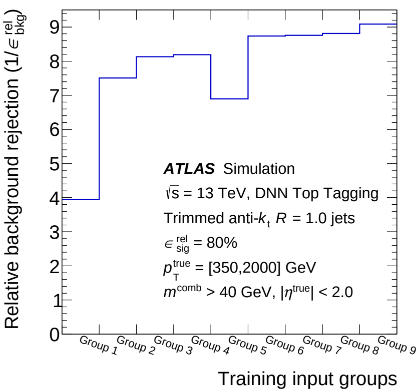

- Different scenarios have been tested by grouping different set of variables.
- The performance of the DNN tagger depends on both the number of variables and the information content in the group.
- Found to be 12 variables for *W*-boson tagging (Group 8) and 13 variables for top-quark tagging (Group 9).

Jet substructure and top tagging

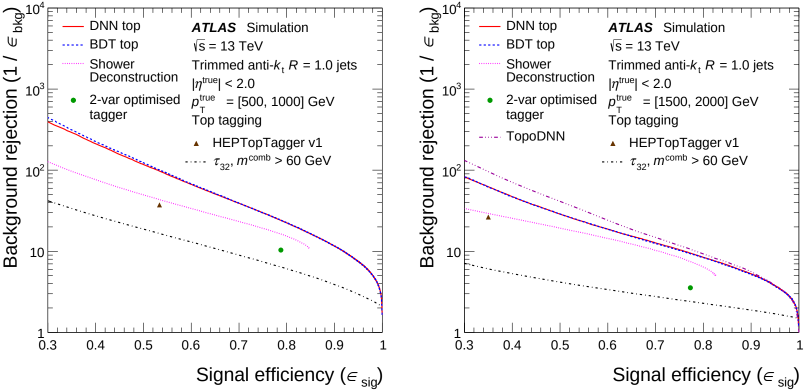

- Similar performance for BDT and DNN multivariate classifiers.
- Large improvement on top-tagging performance by using multivariate classifiers with respect low-level taggers.
- Shower deconstruction (SD) top-tagger better than low-level taggers.
- Worse performance at high p_{T} due to granularity of the calorimeter.

Jet substructure and top tagging

- Performance of the top-tagging studied in data using $t\bar{t}$ events.
  - → One top quark decays hadronically and the other semileptonically in both the electron and the muon decay channels.
  - → b-tagged jet required within the top-candidate large-R jet to ensure $t/\bar{t}$ boosted topologies.

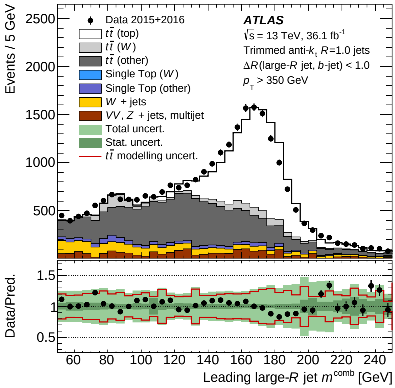

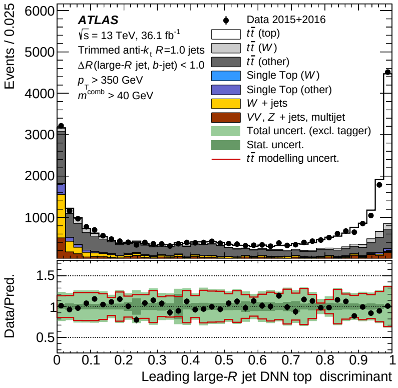

- → Adequate description of the jet mass and DNN score distributions.
- → $t\bar{t}$ modelling uncertainties dominates.

Jet substructure and top tagging

- The performance of top-tagging in the MC is corrected to the one observed in data.
  - → As in the *b*-tagging, this is done using scale factors.
  - → Uncertainties on SD estimated by propagating the uncertainties on the subjet p_{T} to the SD score.
  - → Overall, good agreement on top tagging efficiencies between data and MC across the studied p_{T} range.

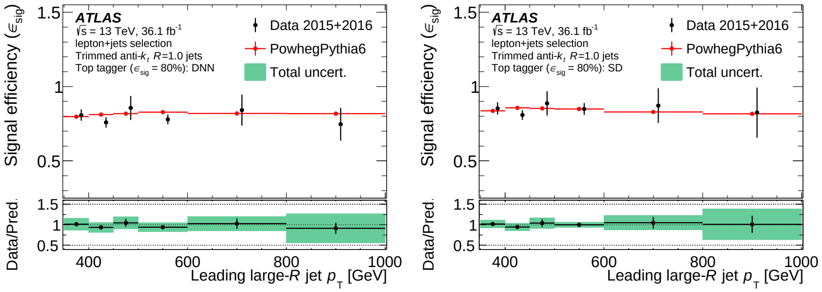

Analysis results: $W' \to$ tb

- Theories beyond the Standard Model (SM) involve enhanced symmetries that predict new gauge bosons, usually called W' or Z' bosons.
- Many models such as those with extra dimensions, strong dynamics, composite Higgs, or the Little Higgs predict new vector charged-current interactions, some with preferential couplings to quarks or third-generation particles.
  - → Sequential Standard Model (SSM) used to capture main phenomenology.
- For large W' masses, decay products of top quark decay become more collimated, such that, the top quark is reconstructed in a single large-R jet.
  - → SD top tagging to identify jets from boosted top-quark decays, whereas b-tagging used to identify jets coming from b-quark.
- Signal bump expected in the top (large-R jet) and b (small-R jet) candidates invariant mass m_{tb}.
- L $= 36.1$ fb^{-1} of data used to perform this search.
  - → Work in progress to include all Run 2 data, L $= 139$ fb^{-1}.

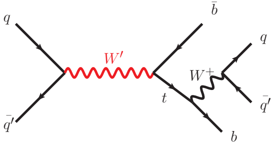

Event reconstruction and selection	
Large-R jet (J)	$p_{\mathrm{T}}^{J} > 420$ GeV, $\lvert\eta\rvert < 2.0$
Small-R jet (j)	$p_{\mathrm{T}}^{j} > 25$ GeV, $\lvert\eta\rvert < 2.5$
Top-quark jet candidate ($J_{\mathrm{top}}^{\mathrm{cand}}$)	jet J with highest $m_j + 0.15 \times m_J$
b-quark jet candidate (j_b^{cand})	highest-p_{T} jet j with $p_{\mathrm{T}}^{j} > 420$ GeV, $\Delta R(J_{\mathrm{top}}^{\mathrm{cand}}, j) > 2.0$
Lepton veto	zero leptons with $p_{\mathrm{T}} > 25$ GeV, $\lvert\eta\rvert < 2.5$
b-quark jet candidate η	zero j_b^{cand} with $\lvert\eta\rvert > 1.2$
0 b-tag in	zero b-tagged jets j with $\Delta R(J_{\mathrm{top}}^{\mathrm{cand}}, j) < 1.0$
1 b-tag in	exactly one b-tagged jet j with $\Delta R(J_{\mathrm{top}}^{\mathrm{cand}}, j) < 1.0$

Analysis results: $W' \to$ tb

- The dominant background from multi-jet production is estimated directly from data using a six-region "2D sideband" method that predicts both the shape and normalisation of $m_{\rm tb}$ distribution.
  - → $N_{\rm A}^{\rm bkg} = R_{\rm A}^{\rm corr} \cdot \frac{(N_{\rm C}^{\rm data} - N_{C}^{t\bar{t}})\cdot(N_{\rm D}^{\rm data} - N_{\rm D}^{t\bar{t}})}{N_{\rm F}^{\rm data} - N_{\rm F}^{t\bar{t}}}$
  - → $N_{\rm B}^{\rm bkg} = R_{\rm B}^{\rm corr} \cdot \frac{(N_{\rm C}^{\rm data} - N_{C}^{t\bar{t}})\cdot(N_{\rm E}^{\rm data} - N_{\rm E}^{t\bar{t}})}{N_{\rm F}^{\rm data} - N_{\rm F}^{t\bar{t}}}$
  - → $R_{\rm A}^{\rm corr}$ and $R_{\rm B}^{\rm corr}$ estimated from MC samples.
- Three ortoghonal signal regions are defined based on top-tagging and b-tagging information.

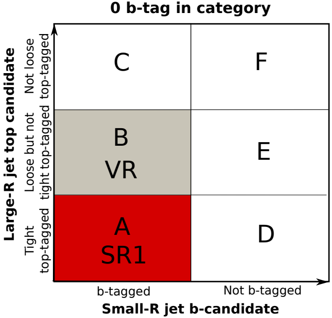

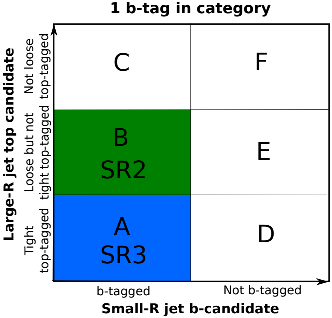

- Several systematic sources taken into account related to jet calibration, b-tagging SFs, top-tagging SFs, multijet background estimation, pile-up and $t\bar{t}$ modelling.

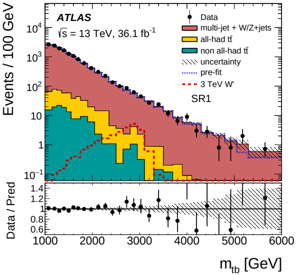

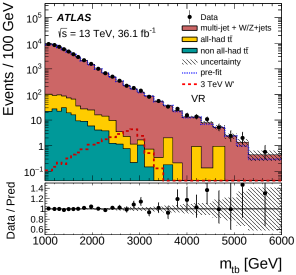

- To test for the presence of a massive resonance, m_{tb} obtained from signal MC and backgrounds are fit to data using a binned maximum-likelihood approach.
- Systematic uncertainties incorporated into the fit as nuisance parameters with log-normal constraints.
- The p_0-value estimated using the log-likelihood ratio (LLR) test statistic.
  - → If no significant excess, upper limits at the 95% CL on the signal production cross-section times branching ratio are derived using the *CLs* method.

- Several systematic sources taken into account related to jet calibration, b-tagging SFs, top-tagging SFs, multijet background estimation, pile-up and $t\bar{t}$ modelling.

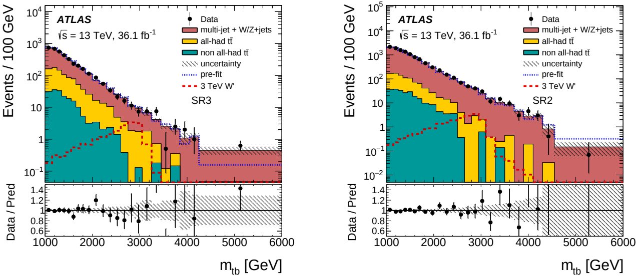

- To test for the presence of a massive resonance, m_{tb} obtained from signal MC and backgrounds are fit to data using a binned maximum-likelihood approach.
- Systematic uncertainties incorporated into the fit as nuisance parameters with log-normal constraints.
- The p_0-value estimated using the log-likelihood ratio (LLR) test statistic.
  - → If no significant excess, upper limits at the 95% CL on the signal production cross-section times branching ratio are derived using the *CLs* method.

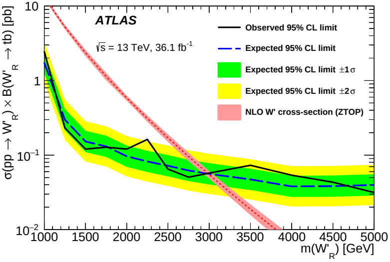

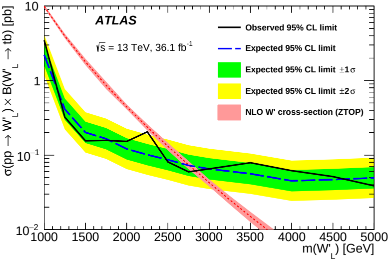

- Exclusion limits derived for right- and left-handed couplings.
- NLO theoretical prediction for W' production computed using ZTOP program.
- For $m(W') \gtrsim 2.0$ TeV, $\sigma \times B > 0.1$ pb excluded.
- Assuming ZTOP parameters (SM couplings), $m(W'_{\mathrm{R}})$ ($m(W'_{\mathrm{L}})$) < 3.0 (2.85) TeV excluded.

Analysis results: $Z' \to b\bar{b}$

- Models favouring couplings fo gauge bosons to third generation quarks in general.
  - → Different models tested in this search: SSM, DM models with Z' mediator, KK resonances.
- $\mathrm{L} = 139\ \mathrm{fb}^{-1}$ of data used to perform this search.
- New *b*-tagging algorithm used for this search: DL1r.
  - → Better performance for high p_{T} jets.
- Signal bump expected in the invariant mass of two leading small-*R* jets.
  - → Both small-*R* jets fulfilling 77% *b*-tagging WP.

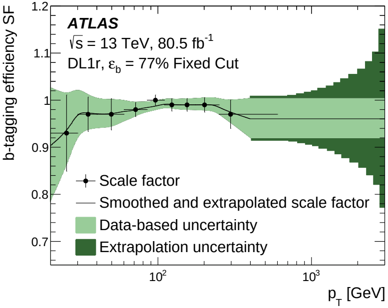

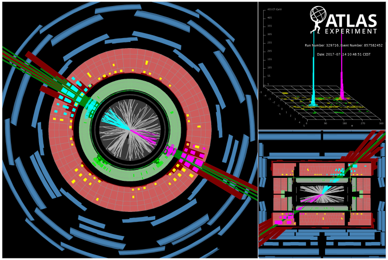

- Event display with two high-p_{T} jets; $p_{\mathrm{T}} = 3.0$ and 2.9 TeV respectively

Analysis results: $Z' \to b\bar{b}$

- SR defined by requiring $|y^*| < 0.8$ → contribution from s-channel enhanced.
- Multijet events main background.
  - → Estimated using sliding-window fitting method using a parametric function: $f(x) = p_1(1-x)^{p_2}x^{p_3+p_4 \log x}$.
  - → $x = m_{jj}/\sqrt{s}$.
  - → Fit validated in a CR with no b-tagging requirement multiplied by the appropiate b-tagging efficiencies.
  - → Signal injection and spurius signal tests performed to evaluate the robustness of the background fitting strategy.
- BumpHunter tool to look for local excesses in the m_{jj} distribution.
  - → No (significant) local excess was found.
- Jet-related and b-tagging uncertainties propagated to signal templates.

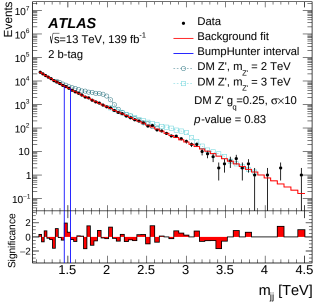

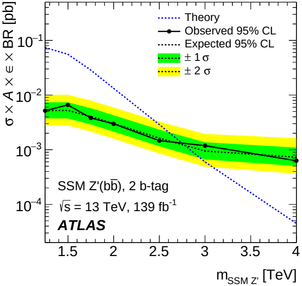

Analysis results: $Z' \to b\bar{b}$

- SR defined by requiring $|y^*| < 0.8 \to$ contribution from s-channel enhanced.
- Multijet events main background.
  - $\to$ Estimated using sliding-window fitting method using a parametric function: $f(x) = p_1(1-x)^{p_2}x^{p_3+p_4 \log x}$.
  - $\to$ $x = m_{jj}/\sqrt{s}$.
  - $\to$ Fit validated in a CR with no b-tagging requirement multiplied by the appropiate b-tagging efficiencies.
  - $\to$ Signal injection and spurius signal tests performed to evaluate the robustness of the background fitting strategy.
- BUMPHUNTER tool to look for local excesses in the m_{jj} distribution.
  - $\to$ No (significant) local excess was found.
- SSM Z' with $m_{Z'} \lesssim 2.8$ TeV excluded.

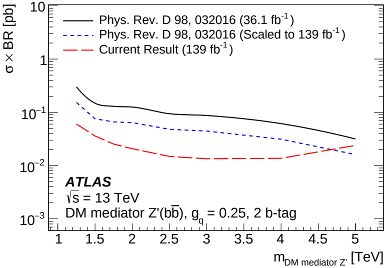

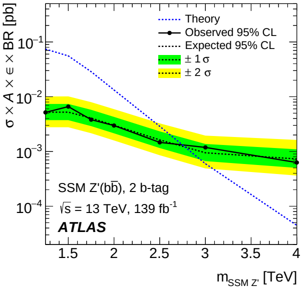

Analysis results: $Z' \rightarrow t\bar{t}$

- Models including heavy resonances decaying into $t\bar{t}$ pair are studied, such as, top-color-assisted-technicolor (TC2), two-Higgs-doublet model (2HDM) and Randall-Sundrum (RS) models of warped extra dimensions.
- For large resonance masses, decay products of top and anti-top quark decays become more collimated, leading to final states with two high p_{T} large-R jets.
  - → DNN top tagging 80% WP is used to identify jets from boosted top and anti-top quark decays.
  - → b-tagging requirements applied to VR trackjets found within large-R jets.
- Signal bump expected in the invariant mass of the top and anti-top large-R jet candidates, $m_{\mathrm{t\bar{t}}}$.
- L $= 139\ \mathrm{fb}^{-1}$ of data used to perform this search.

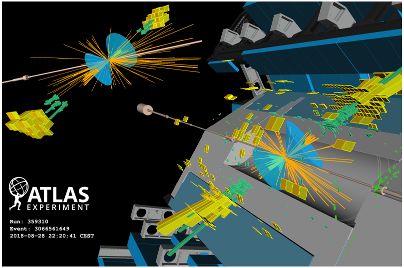

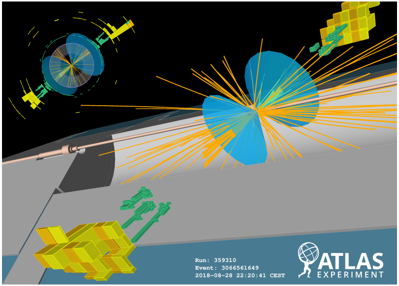

Analysis results: $Z' \to t\bar{t}$

- Two SR are defined depending on the number of b-tagged jets found in the final state ($n_b = 1$ or 2).
  - → For both SRs (SR1b and SR2b) top-candidates must fulfill 80% top tagger WP.
  - → 51% (90%) background contribution from $t\bar{t}$ SM production in SR1b (SR2b)
  - → Remaining background coming from multijet production.
- Background contribution in SRs estimated from fits to parametric function: $f(x) = p_0(1-x)^{p_1} x^{p_2 + p_3 \log\ x + p_4 \log\ x^2}$.
  - → Fitting function validated using the expected $m_{t\bar{t}}$ in SR from a data-driven estimation of multijet contribution and $t\bar{t}$ MC distribution.
  - → Wilk's test to determine the optimal number of parameters to describe the function: most optimal function found for $p_4 = 0.0$.
  - → Spurius signal studies by performing S+B fits on a background only distribution.
- Top tagging SFs plus uncertainties included in the MC predictions.
  - Together with large-R jet related uncertainties, b-tagging uncertainties.
- BUMPHUNTER tool to look for local excesses in the $m_{\mathrm{t\bar{t}}}$ distribution.
  - → No (significant) local excess was found.

- BUMPHUNTER tool to look for local excesses in the $m_{t\bar{t}}$ distribution.
  - → No (significant) local excess was found.
  - → Global p-values of 0.45 and 0.56 for SR1b and SR2b respectively.
  - → Local excesses less than 2-σ away from the SM prediction.
- Exclusion limits at 95% CL performed using a test statistic based on the profile likelihood ratio.

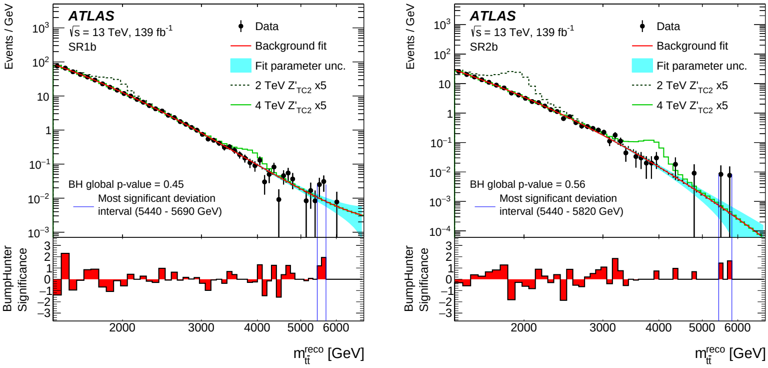

Analysis results: $Z' \to t\bar{t}$

- Signal bump expected in the invariant mass of the top and anti-top large-*R* jet candidates, $m_{t\bar{t}}$.
  - → No (significant) local excess was found.
  - → Global p-values of 0.45 and 0.56 for SR1b and SR2b respectively.
  - → Local excesses less than 2-σ away from the SM prediction.
- Exclusion limits at 95% CL performed using a test statistic based on the profile likelihood ratio.
  - → Limits on topcolor-assisted-technicolor model, resulting in the exclusion of Z' masses up to 3.9 and 4.9 TeV for decay widths of 1% and 3%, respectively.

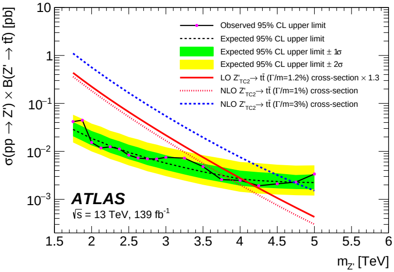

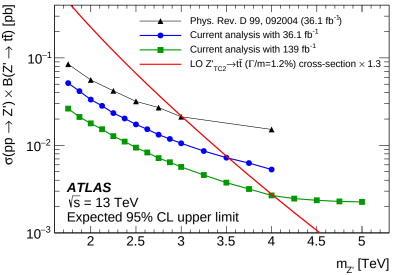

Conclusions

- Searches for heavy resonances decaying into third generation quarks have been presented.
  - → $W' \to tb$ with $\mathrm{L} = 36.1$ fb^{-1}; SSM m(W'_R) (m(W'_L)) < 3.0 (2.85) TeV excluded.
  - → $Z' \to b\bar{b}$ with $\mathrm{L} = 139$ fb^{-1}; SSM m(Z') < 2.8 TeV excluded.
  - → $Z' \to t\bar{t}$ with $\mathrm{L} = 139$ fb^{-1}; SSM m(Z'_TC2) < 3.9 (4.9) TeV excluded for $\Gamma/m = 1\%$ (3%)
- In general, these limits on $m_{W',Z'}$ are relaxed by assuming smaller couplings to SM quarks.
  - → Is there any deep reason to assume $g_{q\bar{q}V'} \approx g_{q\bar{q}V}^{\mathrm{SM}}$?. I guess this will depend on the particular theoretical model ...
  - → 2D limits ($m_{W'}$,g') searching for $W' \to tb$ using the leptonic decay of the top.
- New techniques included in the b-tagging and top-tagging algorithms.
  - → Better performance compared to the low level algorithms.
  - → Important to be able to properly compute the systematic uncertainties associated to these new WPs.
- A lot of work done in the performance size for a thoroughly estimation of the systematic uncertainties and its correlations associated to jets, top-tagging and b-tagging.
  - → Important role in the profile likelihood fit.
  - → A measurement must be always accompanied by its error.

Thank you

Backup

$W' \to tb$ leptonic channel